Quantum detector tomography of a time-multiplexed superconducting nanowire single-photon detector at telecom wavelengths

Chandra M. Natarajan,[1,2,*] Lijian Zhang,[3,4] Hendrik Coldenstrodt-Ronge,[3] Gaia Donati,[3] Sander N. Dorenbos,[5] Val Zwiller,[5] Ian A. Walmsley,[3] and Robert H. Hadfield[1,6]

[1]*School of Engineering and Physical Sciences, Heriot-Watt University, Edinburgh EH14 4AS, UK*
[2]*Current address: Ginzton laboratory, Stanford University, Stanford, California, 94305, USA*
[3]*Clarendon Laboratory, Oxford University, Parks Road, Oxford, OX1 3PU, UK*
[4]*Current address: Max Planck Research Department for Structural Dynamics at the University of Hamburg, Building 99, Luruper Chaussee 149, 22761 Hamburg, Germany*
[5]*Kavli Institute of Nanoscience, Delft University of Technology, 2628 CJ Delft, The Netherlands*
[6]*Current address: School of Engineering, University of Glasgow, Glasgow, G12 8QQ, UK*
**cmn@stanford.edu*

Abstract: Superconducting nanowire single-photon detectors (SNSPDs) are widely used in telecom wavelength optical quantum information science applications. Quantum detector tomography allows the positive-operator-valued measure (POVM) of a single-photon detector to be determined. We use an all-fiber telecom wavelength detector tomography test bed to measure detector characteristics with respect to photon flux and polarization, and hence determine the POVM. We study the SNSPD both as a binary detector and in an 8-bin, fiber based, Time-Multiplexed (TM) configuration at repetition rates up to 4 MHz. The corresponding POVMs provide an accurate picture of the photon number resolving capability of the TM-SNSPD.

OCIS codes: (040.5570) Quantum detectors; (270.5570) Quantum detectors; (270.5585) Quantum information and processing.

References

1. D. T. Smithey, M. Beck, M. G. Raymer, and A. Faridani, "Measurement of the Wigner distribution and the density matrix of a light mode using optical homodyne tomography: application to squeezed states and the vacuum," Phys. Rev. Lett. **70**(9), 1244–1247 (1993).
2. J. F. Poyatos, J. I. Cirac, and P. Zoller, "Complete characterization of a quantum process: The two-bit quantum gate," Phys. Rev. Lett. **78**(2), 390–393 (1997).
3. J. S. Lundeen, A. Feito, H. Coldenstrodt-Ronge, K. L. Pregnell, C. Silberhorn, T. C. Ralph, J. Eisert, M. B. Plenio, and I. A. Walmsley, "Tomography of quantum detectors," Nat. Phys. **5**(1), 27–30 (2009).
4. A. Luis and L. L. Sanchez-Soto, "Complete characterization of arbitrary quantum measurement processes," Phys. Rev. Lett. **83**(18), 3573–3576 (1999).
5. J. Fiurášek, "Maximum-likelihood estimation of quantum measurement," Phys. Rev. A **64**(2), 024102 (2001).
6. G. M. D'Ariano, L. Maccone, and P. Lo Presti, "Quantum calibration of measurement instrumentation," Phys. Rev. Lett. **93**(25), 250407 (2004).
7. H. B. Coldenstrodt-Ronge, J. S. Lundeen, K. L. Pregnell, A. Feito, B. J. Smith, W. Mauerer, C. Silberhorn, J. Eisert, M. B. Plenio, and I. A. Walmsley, "A proposed testbed for detector tomography," J. Mod. Opt. **56**(2-3), 432–441 (2009).
8. G. Brida, L. Ciavarella, I. P. Degiovanni, M. Genovese, L. Lolli, M. G. Mingolla, F. Piacentini, M. Rajteri, E. Taralli, and M. G. A. Paris, "Quantum characterization of superconducting photon counters," New J. Phys. **14**(8), 085001 (2012).
9. M. A. Itzler, X. D. Jiang, M. Entwistle, K. Slomkowski, A. Tosi, F. Acerbi, F. Zappa, and S. Cova, "Advances in InGaAsP-based avalanche diode single photon detectors," J. Mod. Opt. **58**(3-4), 174–200 (2011).
10. A. E. Lita, A. J. Miller, and S. W. Nam, "Counting near-infrared single-photons with 95% efficiency," Opt. Express **16**(5), 3032–3040 (2008).

#175855 - $15.00 USD Received 10 Sep 2012; revised 18 Dec 2012; accepted 18 Dec 2012; published 9 Jan 2013

11. D. Rosenberg, A. E. Lita, A. J. Miller, and S. W. Nam, "Noise-free high-efficiency photon-number-resolving detectors," Phys. Rev. A **71**(6), 061803 (2005).
12. C. M. Natarajan, M. G. Tanner, and R. H. Hadfield, "Superconducting nanowire single-photon detectors: physics and applications," Supercond. Sci. Technol. **25**(6), 063001 (2012).
13. R. H. Hadfield, "Single-photon detectors for optical quantum information applications," Nat. Photonics **3**(12), 696–705 (2009).
14. M. D. Eisaman, J. Fan, A. Migdall, and S. V. Polyakov, "Invited review article: Single-photon sources and detectors," Rev. Sci. Instrum. **82**(7), 071101 (2011).
15. H. Takesue, S. W. Nam, Q. Zhang, R. H. Hadfield, T. Honjo, K. Tamaki, and Y. Yamamoto, "Quantum key distribution over a 40-dB channel loss using superconducting single-photon detectors," Nat. Photonics **1**(6), 343–348 (2007).
16. C. M. Natarajan, A. Peruzzo, S. Miki, M. Sasaki, Z. Wang, B. Baek, S. Nam, R. H. Hadfield, and J. L. O'Brien, "Operating quantum waveguide circuits with superconducting single-photon detectors," Appl. Phys. Lett. **96**(21), 211101 (2010).
17. R. H. Hadfield, M. J. Stevens, S. S. Gruber, A. J. Miller, R. E. Schwall, R. P. Mirin, and S. W. Nam, "Single photon source characterization with a superconducting single photon detector," Opt. Express **13**(26), 10846–10853 (2005).
18. K. De Greve, L. Yu, P. L. McMahon, J. S. Pelc, C. M. Natarajan, N. Y. Kim, E. Abe, S. Maier, C. Schneider, M. Kamp, S. Höfling, R. H. Hadfield, A. Forchel, M. M. Fejer, and Y. Yamamoto, "Quantum-dot spin-photon entanglement via frequency downconversion to telecom wavelength," Nature **491**(7424), 421–425 (2012).
19. V. D'Auria, N. Lee, T. Amri, C. Fabre, and J. Laurat, "Quantum decoherence of single-photon counters," Phys. Rev. Lett. **107**(5), 050504 (2011).
20. L. J. Zhang, H. B. Coldenstrodt-Ronge, A. Datta, G. Puentes, J. S. Lundeen, X. M. Jin, B. J. Smith, M. B. Plenio, and I. A. Walmsley, "Mapping coherence in measurement via full quantum tomography of a hybrid optical detector," Nat. Photonics **6**(6), 364–368 (2012).
21. M. K. Akhlaghi, A. H. Majedi, and J. S. Lundeen, "Nonlinearity in single photon detection: modeling and quantum tomography," Opt. Express **19**(22), 21305–21312 (2011).
22. J. J. Renema, G. Frucci, Z. Zhou, F. Mattioli, A. Gaggero, R. Leoni, M. J. A. de Dood, A. Fiore, and M. P. van Exter, "Modified detector tomography technique applied to a superconducting multiphoton nanodetector," Opt. Express **20**(3), 2806–2813 (2012).
23. D. Achilles, C. Silberhorn, C. Sliwa, K. Banaszek, and I. A. Walmsley, "Fiber-assisted detection with photon number resolution," Opt. Lett. **28**(23), 2387–2389 (2003).
24. A. Feito, J. S. Lundeen, H. Coldenstrodt-Ronge, J. Eisert, M. B. Plenio, and I. A. Walmsley, "Measuring measurement: theory and practice," New J. Phys. **11**(9), 093038 (2009).
25. L. Zhang, A. Datta, H. B. Coldenstrodt-Ronge, X.-M. Jin, J. Eisert, M. B. Plenio, and I. A. Walmsley, "Recursive quantum detector tomography," New J. Phys. **14**(11), 115005 (2012).
26. G. N. Gol'tsman, O. Okunev, G. Chulkova, A. Lipatov, A. Semenov, K. Smirnov, B. Voronov, A. Dzardanov, C. Williams, and R. Sobolewski, "Picosecond superconducting single-photon optical detector," Appl. Phys. Lett. **79**(6), 705–707 (2001).
27. A. D. Semenov, G. N. Gol'tsman, and A. A. Korneev, "Quantum detection by current carrying superconducting film," Physica C **351**(4), 349–356 (2001).
28. J. K. W. Yang, A. J. Kerman, E. A. Dauler, V. Anant, K. M. Rosfjord, and K. K. Berggren, "Modeling the electrical and thermal response of superconducting nanowire single-photon detectors," IEEE Trans. Appl. Supercond. **17**(2), 581–585 (2007).
29. A. Divochiy, F. Marsili, D. Bitauld, A. Gaggero, R. Leoni, F. Mattioli, A. Korneev, V. Seleznev, N. Kaurova, O. Minaeva, G. Gol'tsman, K. G. Lagoudakis, M. Benkhaoul, F. Levy, and A. Fiore, "Superconducting nanowire photon-number-resolving detector at telecommunication wavelengths," Nat. Photonics **2**(6), 302–306 (2008).
30. S. Jahanmirinejad, G. Frucci, F. Mattioli, D. Sahin, A. Gaggero, R. Leoni, and A. Fiore, "Photon-number resolving detector based on a series array of superconducting nanowires," Appl. Phys. Lett. **101**(7), 072602 (2012).
31. M. J. Stevens, B. Baek, E. A. Dauler, A. J. Kerman, R. J. Molnar, S. A. Hamilton, K. K. Berggren, R. P. Mirin, and S. W. Nam, "High-order temporal coherences of chaotic and laser light," Opt. Express **18**(2), 1430–1437 (2010).
32. S. N. Dorenbos, E. M. Reiger, U. Perinetti, V. Zwiller, T. Zijlstra, and T. M. Klapwijk, "Low noise superconducting single photon detectors on silicon," Appl. Phys. Lett. **93**(13), 131101 (2008).
33. R. Radebaugh, "Refrigeration for superconductors," Proc. IEEE **92**(10), 1719–1734 (2004).
34. K. Banaszek and I. A. Walmsley, "Photon counting with a loop detector," Opt. Lett. **28**(1), 52–54 (2003).
35. V. Anant, A. J. Kerman, E. A. Dauler, J. K. W. Yang, K. M. Rosfjord, and K. K. Berggren, "Optical properties of superconducting nanowire single-photon detectors," Opt. Express **16**(14), 10750–10761 (2008).
36. S. N. Dorenbos, E. M. Reiger, N. Akopian, U. Perinetti, V. Zwiller, T. Zijlstra, and T. M. Klapwijk, "Superconducting single photon detectors with minimized polarization dependence," Appl. Phys. Lett. **93**(16), 161102 (2008).
37. M. Tinkham, *Introduction to superconductivity* (McGraw-Hill, 1996)
38. M. G. Tanner, C. M. Natarajan, V. K. Pottapenjara, J. A. O'Connor, R. J. Warburton, R. H. Hadfield, B. Baek, S. Nam, S. N. Dorenbos, E. B. Urena, T. Zijlstra, T. M. Klapwijk, and V. Zwiller, "Enhanced telecom wavelength

#175855 - $15.00 USD Received 10 Sep 2012; revised 18 Dec 2012; accepted 18 Dec 2012; published 9 Jan 2013

single-photon detection with NbTiN superconducting nanowires on oxidized silicon," Appl. Phys. Lett. **96**(22), 221109 (2010).
39. J. Řeháček, D. Mogilevtsev, and Z. Hradil, "Tomography for quantum diagnostics," New J. Phys. **10**(4), 043022 (2008).
40. K. M. R. Audenaert and S. Scheel, "Quantum tomographic reconstruction with error bars: a Kalman filter approach," New J. Phys. **11**(2), 023028 (2009).

1. Introduction

Experiments in quantum information science (QIS) typically encompass quantum state preparation, quantum operation (process) and quantum measurement. A carefully designed trial requires detailed information on each of these stages. Quantum tomography techniques have been developed to extract complete descriptions of these individual stages [1–3]. Quantum state tomography gives a detailed picture of the input states [1]; quantum process tomography is used to characterize operations, such as the function of quantum logic gates [2] and quantum detector tomography (QDT) allows reconstruction of the positive operator-valued measure (POVM) elements [3–8] of a measurement apparatus. This article will focus on QDT for photodetection: using coherent input states, the statistics of the measurement outputs reveal complete information about the photon-counting detector.

In optical QIS, photons are used as flying quantum bits ('qubits'). Highly efficient, low noise single-photon detectors at the desired wavelength are essential. Recently, QDT of a silicon single-photon avalanche photodiode (SPAD) was demonstrated by reconstructing the POVM elements for a binary (click / no click) detector and also for a Time-Multiplexed (TM) detector with photon number resolving (PNR) capability [3]. Si-SPADs are only suitable for use at visible and near infrared wavelengths. For experiments at technologically-important telecom wavelengths the main contending technologies are InGaAs SPADs [9], superconducting Transition Edge Sensors (TESs) [10, 11] or Superconducting Nanowire Single-Photon Detectors (SNSPDs/SSPDs) [12]. InGaAs SPADs compared to Si SPADs have greatly elevated dark count rates, making gating essential. TESs offer near unity efficiency with PNR capability, but require sub-Kelvin operating temperatures. SNSPDs operate at a more accessible temperature (~4 K) offering free-running single-photon sensitivity from visible to mid infrared with low dark counts (1-100 Hz), excellent timing resolution (< 60 ps) and short dead time (~10 ns) [12–14]. These properties have enabled SNSPDs to be widely used in QIS applications such as quantum key distribution [15], characterization of quantum circuits [16], characterization of single photon sources [17] and development of quantum repeaters via spin-photon entanglement [18]. Typically SNSPDs are characterized semi-classically: the detection efficiency and dark count rate are extracted from a measurement of counts as a function of photon flux; by altering the biasing conditions the relationship between detection efficiency and dark count rate can be determined [12]. The QDT technique allows a complete characterization of a quantum detector, therefore offers the opportunity to reveal nonclassical features of the detector [19, 20]. Recently QDT has been performed on a SNSPD in the non-linear regime, which requires the SNSPD to be biased much lower than their critical current ($I_{bias} << I_{critical}$), to characterize multi-photon sensitivity [21, 22]. In this regime the efficiency of the SNSPD is very low. We have taken an alternate route to report the PNR characteristics of SNSPDs in the linear regime by using the time-multiplexing technique [23]. We have constructed an all-fiber QDT setup to characterize the individual SNSPDs as well as a fiber based time-multiplexed (TM) photon number resolving SNSPD network. Two highly efficient fiber-coupled SNSPDs (system detection efficiency (SDE) > 20% at 1310 nm; SDE > 10% at 1550 nm) were used to construct an 8-bin TM-SNSPD and operated at 1 - 4 MHz clock rate at telecom wavelengths.

2. Quantum detector tomography

A quantum non-projective measurement device in a quantum mechanical setup is mathematically described by positive operator-valued measure (POVM) formalism. The

#175855 - $15.00 USD Received 10 Sep 2012; revised 18 Dec 2012; accepted 18 Dec 2012; published 9 Jan 2013

POVM elements $\{\pi_n\}$ are extracted from the detection probability, $p_{n,\rho}$, for an input state ρ from equation $p_{n,\rho} = tr[\rho\pi_n]$. Reconstructing π_n from $p_{n,\rho}$ is the objective in quantum detector tomography, whilst maintaining $\pi_n \geq 0$, semi-definite such that $\sum_n \pi_n = I$ for a physical detector. A *d*-dimensional Hilbert space is used to reconstruct the POVM elements. The input or probe states are prepared to form a set $\{\rho_j\}$, which is tomographically complete, to extract π_n [3, 24]. Coherent states $|\alpha\rangle$ form an overcomplete basis for the Hilbert space upon which the photodetection operates. Further, they are simpler to prepare than pure number states. In our experiment the probe states are reliably and easily generated using a diode laser. A general quantum detector may have phase-sensitivity. The corresponding tomography procedure for the reconstruction of the full POVM matrices therefore requires both amplitude and phase modulation of the probe states as well as a special reconstruction algorithm [24, 25]. The situation discussed in this article has been simplified: due to the absence of a phase reference the SNSPDs are assumed to be phase-insensitive therefore only the diagonal elements of the POVM matrices have been reconstructed. The tomographically complete set of input states $\{|\alpha\rangle\langle\alpha|\}$ is prepared by varying the amplitude α by means of a pair of calibrated commercial variable optical attenuators. The amplitude of the coherent states have been chosen such that the detection probability is high enough to complete the measurements within a reasonable time interval. The entire experimental setup is based on single-mode fiber (from source to detector), which allows the assumption that the device detects the same single-mode coherent states as generated by the laser. An ideal detector output $\frac{1}{\pi}\langle\alpha|\pi_n|\alpha\rangle$ contains the information of the POVM elements. The diagonal components of the representation of the POVM elements in the number basis (Eq. (1).) describes a simplified practical detector without phase sensitivity.

$$\pi_n = \sum_{k=0}^{\infty} \theta_k^{(n)} |k\rangle\langle k|. \tag{1}$$

The equation can be modified to a finite matrix form $P = F\Pi$ by truncating to *M* number states. $P_{D\times N}$ contains the measured statistics of an N-outcome detector and $F_{D\times M}$ contains the *D* probe states $\{\alpha_0, \alpha_1, ..., \alpha_n\}$, $\Pi_{M\times N}$ contains the POVM. The physical POVM is obtained by solving the optimization problem $\min\{\|P - F\Pi\|_2 + g(\Pi)\}$, where $\|A\|_2$ is defined as $\left(\sum_{i,j} |A_{i,j}|^2\right)^{1/2}$, and $g(\Pi)$ is a regularization condition to suppress any potential ill-conditioning of the reconstruction [24].

3. Superconducting nanowire single-photon detectors (SNSPDs)

3.1 SNSPD operating principle

A niobium nitride (NbN) superconducting nanowire (200 nm wide, 5 nm thick) maintained well below its critical temperature and direct current (DC) biased just below the critical current was shown to be sensitive to single photons by Gol'tsman and associates in 2001 [26]. This device is known as the superconducting single-photon detector (SSPD) or superconducting nanowire single-photon detector (SNSPD) [12]. SNSPDs operate at a temperature ~4 K, and so can be cooled straightforwardly using liquid helium or closed-cycle refrigeration. When a photon is absorbed by the current-biased superconducting nanowire a small resistive hotspot is created. The supercurrent is diverted around the periphery of the hotspot. As the hotspot grows, the local current density around the hotspot increases,

#175855 - $15.00 USD Received 10 Sep 2012; revised 18 Dec 2012; accepted 18 Dec 2012; published 9 Jan 2013

exceeding the superconducting critical current density. This in turn leads to the formation of a resistive barrier across the width of the nanowire. The resistive hotspot further grows along the axis of the nanowire due to Joule heating. This generates a measurable voltage across the SNSPD. It was conjectured that by studying the hotspot resistances, it would be possible to reveal the number of photons absorbed by the nanowire [27]. Recently however, it was demonstrated that the Joule heating of the nanowire suppresses the initial variation in the hotspot resistances due to multiple photon events [28]. Nevertheless, photon number resolution can still be realized if the device is biased low enough that a multiphoton event is necessary to trigger a switch from the superconducting- to normal state [21, 22, 26]. It should be noted that the triggering probability is very low in this mode of operation. Alternately, photon number resolution can be achieved in SNSPDs by spatial multiplexing (using multiple pixels) [29–31] or by time multiplexing (this article, § 3.3). In summary, a SNSPD, biased close to its critical current, exhibits a binary behavior by outputting an electronic pulse (1-click) or none (no-click) in the presence or absence of photon(s). In this basic scenario, the SNSPD cannot recognize the number of photons present at the input mode and does not possess PNR capability.

3.2 Binary SNSPDs

The SNSPDs used in this study are based on an NbTiN nanowire on a Si substrate with a 225 nm SiO_2 layer [32]. The SiO_2/Si interface beneath the nanowire enhances the absorption of telecom wavelength photons, giving peak detection efficiency at 1310 nm wavelength. The 100 nm wide nanowire meanders across an area covering 10 μm × 10 μm with a 50% fill factor. The devices were maintained at 2.8 K, well below the observed device superconducting transition temperature of 8 K, in a Gifford–McMahon closed cycle refrigerator [17, 33]. The detectors were aligned individually to a single-mode telecom optical fiber (9 μm mode field diameter at 1550 nm). The schematic of the experimental setup for the tomography experiment on a binary SNSPD is shown in Fig. 1. The single-mode coherent states are generated by a fiber coupled diode laser. In order to ensure that the detectors are memoryless, the laser diode was gain switched, using a pulse pattern generator, such that the wavepackets were preceded and followed by time intervals with no input light. The SNSPDs have a deadtime of roughly 10-20 ns, i.e. the time during which the SNSPD is insensitive to the incoming probe state. The laser output is split using a 1:99 fiber beamsplitter to monitor the optical power during the experiment. The 1% fraction of the laser output is further attenuated to reach the single-photon regime using two individually calibrated programmable fiber attenuators. The polarization of the photons reaching the detector is controlled by a fiber-polarizer. The output of the SNSPD is amplified using commercial room temperature amplifiers (RF Bay LNA 580 & 1000), converted to a logic pulse via a pulse generator (Agilent 81110A) and read out via a custom Field Programmable Gate Array (FPGA) unit.

#175855 - $15.00 USD Received 10 Sep 2012; revised 18 Dec 2012; accepted 18 Dec 2012; published 9 Jan 2013

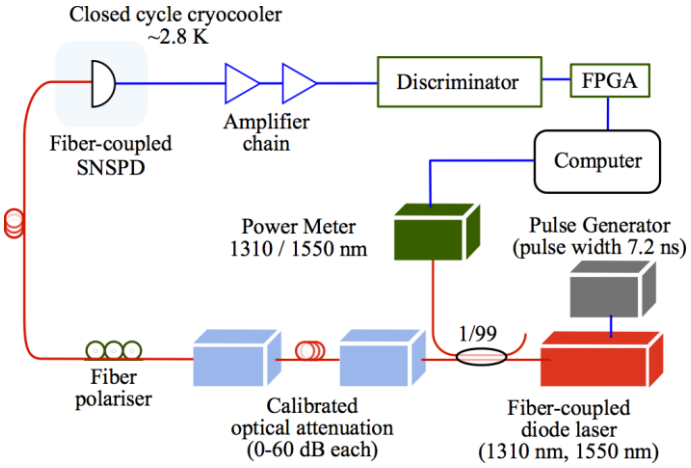

Fig. 1. The experimental setup for the tomography experiment for a binary SNSPD.

3.3 Time multiplexed SNSPDs

Any conventional binary single photon detector (such as a Si APD) can be granted photon number resolution by constructing a time-multiplexing fiber network (as in Fig. 2(a)) [23, 34]. The time multiplexing scheme splits the input pulse, contained in a single temporal mode (or time-bin) into many time-bins using beamsplitters and temporal delays. This results in a reduced probability of having more than one photon per time bin. The outputs of the fiber network are monitored with twin SNSPDs. Summation of the number of clicks from both detectors for a particular input pulse will result in photon number resolution. In this study, a 9-outcome (0 - 8 clicks) Time-Multiplexed SNSPD (TM-SNSPD) was implemented using fiber-network with 8 time bins (4 time bins in 2 arms) with two SNSPDs operating in their linear detection regime coupled to the outputs. The fibers and beamsplitters were chosen such that the TM-SNSPD can be operated in the telecom wavelength range (1310 nm and 1550 nm). The TM-SNSPD splits the input wavepacket into time bins spread over 90 ns. The SNSPDs used in these experiments are assumed to be memory-less and therefore delays between subsequent measurements on the SNSPD have been incorporated to accommodate for the dead time of the detector (20 ns). A snapshot oscilloscope trace of one SNSPD with four successive clicks in each time bin is shown in Fig. 2(b). The inverse of the total time bin interval limits the maximum rate at which the TM-SNSPD can be run. The experimental results presented have been recorded at a maximum rate of 4 MHz (limited by the dead time of the FPGA readout electronics).

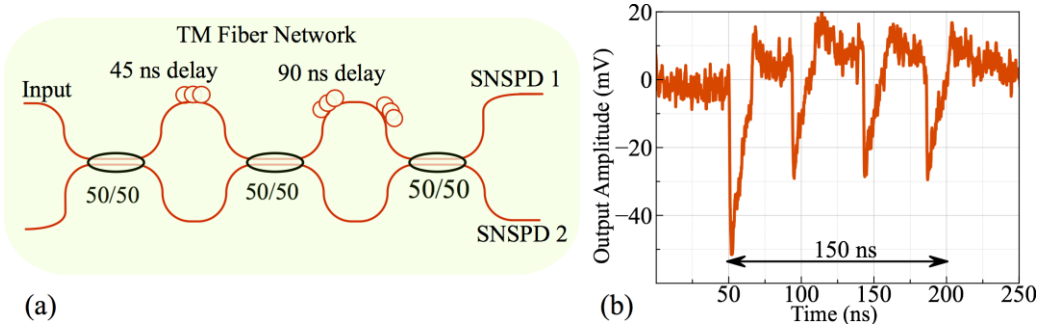

Fig. 2. (a) Time-multiplexed (TM) fiber network for photon number resolving single photon detection [23]. A pair of SNSPDs is implemented at the outputs to create a TM-SNSPD. (b) An oscilloscope trace showing the output pulses from one of the SNSPDs in the TM detector, the optical pulse split is over 4 time bins in each path.

#175855 - $15.00 USD Received 10 Sep 2012; revised 18 Dec 2012; accepted 18 Dec 2012; published 9 Jan 2013

4. Results

4.1 Bias current dependence

The operating principle of the SNSPDs (§ 3.1) confirms that the sensitivity of the SNSPD depends on the bias current (I_b) of the device. The nonlinearity of the SNSPD has been demonstrated previously at low bias points [21]. In our current study, the device has been current biased at different bias points ($I_b = v \times I_c$) where I_c is the critical current of the device and values of v were chosen as 0.7 and 0.9. The polarization of the incoming optical pulse (λ = 1550 nm at a repetition rate of 1 MHz) was set to a constant angle with respect to the nanowire orientation such that the detected counts were maximized (polarization dependence of SNSPD is discussed in § 4.2). The measured statistics for the number of registered clicks (0 or 1) on the binary SNSPD is plotted in Fig. 3(a). The common observation that the sensitivity of the nanowire increases with I_b. The measured statistics of the TM-SNSPD for v = 0.9 is shown in Fig. 3(b). The POVM elements $\{\pi_n\}$ for n-clicks reconstructed from measured statistics are shown in Fig. 3(c) and Fig. 3(d). We assume the off-diagonal elements are zero for these detectors (TM and binary). The diagonal elements are plotted in Fig. 3(c) and Fig. 3(d) for v = 0.7 and v = 0.9.

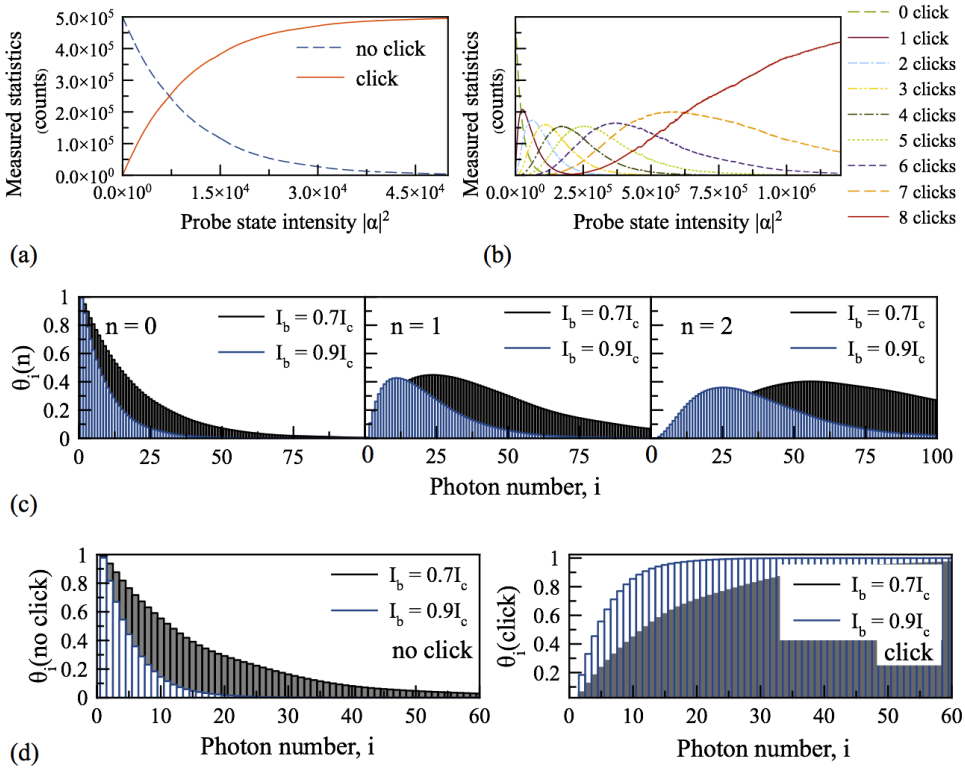

Fig. 3. (a) The measured statistics of click and no click from a SNSPD binary detector operating at 1550 nm wavelength at a repetition rate of 1 MHz. The data acquisition time was 0.5 seconds/point. (b) The measured statistics from a TM-SNSPD detector for 0-8 clicks at λ = 1550 nm operating at 1 MHz repetition rate. The data acquisition time was 0.5 seconds/point. (c) Diagonal elements of the reconstructed POVM elements for clicks 0, 1, 2 from a TM-SNSPD at λ = 1550 nm. The shaded bar represents bias point 0.7 × I_C and the unshaded bar represents 0.9 × I_C . (d) diagonal elements of the reconstructed POVM elements for clicks 0 and 1 for a binary-SNSPD is plotted at λ = 1550 nm. The shaded bars represent the bias point 0.7 × I_C and the unshaded bars represent 0.9 × I_C.

#175855 - $15.00 USD Received 10 Sep 2012; revised 18 Dec 2012; accepted 18 Dec 2012; published 9 Jan 2013

4.2 Polarization dependence

The SNSPD has been observed to possess noticeable polarization sensitivity due to the geometry of the device [35, 36]. The meander structure is essentially a subwavelength grating (as shown in Fig. 4(a)) It has been reported that the count rate from the detector displays a maximum and a minimum value depending on the orientation of the electric field being either parallel or perpendicular to the orientation of the nanowire. This is because of the variation in absorption exhibited by the meander structure depending on the polarization [35]. The polarization dependence is observed by varying the polarization of the incident photons using a fiber polarizer. The dimensionality of the Hilbert space has to be increased to include the polarization sensitivity of the device. However to make the experiment simpler the POVM elements are extracted for just two polarization states of incident photons with respect to the nanowire orientation. At telecom wavelengths the detection efficiency is maximized (minimized) when the electric field is polarized parallel (perpendicular) to the length of the nanowire segments. Fiber polarizers are adjusted to either high or low count rate and corresponding output statistics are measured. The variation in POVM elements (diagonal elements) observed is plotted in Fig. 4(b) (binary detector) and Fig. 4(c) (TM-SNSPD) for two polarization states at $\lambda = 1550$ nm measured at 1 MHz repetition rate.

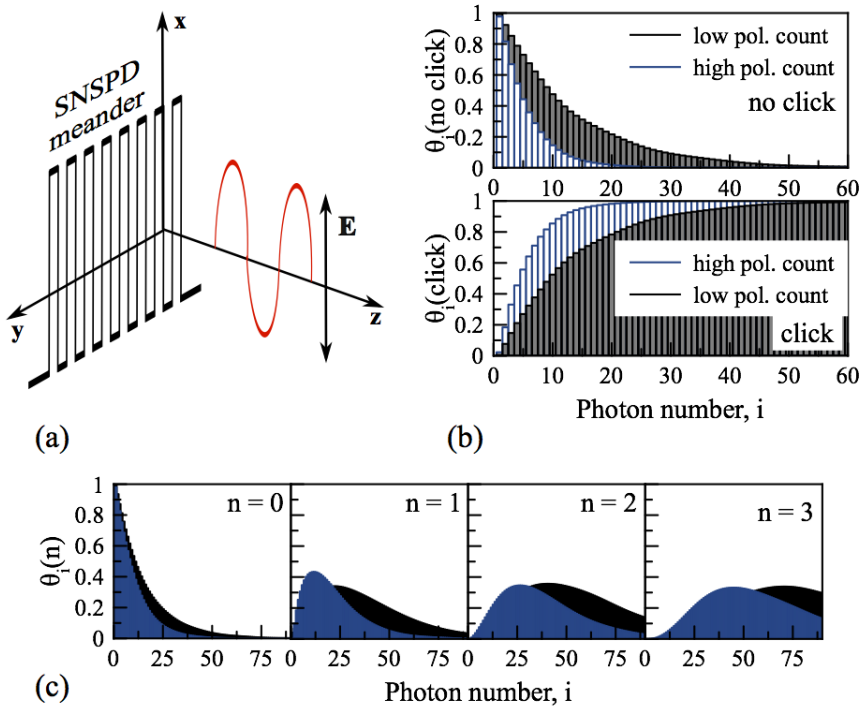

Fig. 4. (a) A schematic to represent the orientation of the electric field, ***E*** of the optical illumination with respect to the SNSPD meander geometry. The detection efficiency is maximized when the electric field is polarized along the length of the nanowire segments (x-direction) (b) Diagonal elements of the reconstructed POVM elements for clicks 0 and 1 from a binary SNSPD (biased at $0.9 \times I_C$) at $\lambda = 1550$ nm are plotted. The shaded graph represents low polarization counts and the unshaded graph represents high polarization counts. (c) Diagonal elements of the reconstructed POVM elements for clicks 0, 1, 2 and 3 from a TM-SNSPD (biased at $0.9 \times I_C$) at $\lambda = 1550$ nm. In each case the blue graph represents high polarization counts and the black graph represents low polarization counts.

#175855 - $15.00 USD Received 10 Sep 2012; revised 18 Dec 2012; accepted 18 Dec 2012; published 9 Jan 2013

4.3 Wavelength dependence

One of the features of the SNSPD is its exceptionally broad spectral range: the sensitivity of the SNSPD is ultimately only limited by the BCS superconducting energy gap of the nanowire (~meV in a material such as NbTiN) [37]. In practice however, in ambient conditions, the wavelength of room temperature black body photons (~10 μm wavelength, corresponding to an energy of ~0.12 eV) is a realistic cut off. The spectral dependence of the SNSPD device efficiency is also influenced by the device architecture. As described in § 3.2, the SNSPDs used in this experiment each consist of an NbTiN nanowire on a Si substrate with a 225 nm SiO_2 layer in between [32]. The SiO_2/Si interface acts as a mirror due to the refractive index mismatch. This 225nm SiO_2 layer matches the optical thickness of $\lambda/4$ at λ = 1310 nm thus giving an electric field maximum at the NbTiN layer; correspondingly the best efficiency for these SNSPDs is found at this wavelength [38]. The extracted diagonal components of the POVM elements have been plotted in Fig. 5 for λ = 1310 nm at repetition rate of 4 MHz.

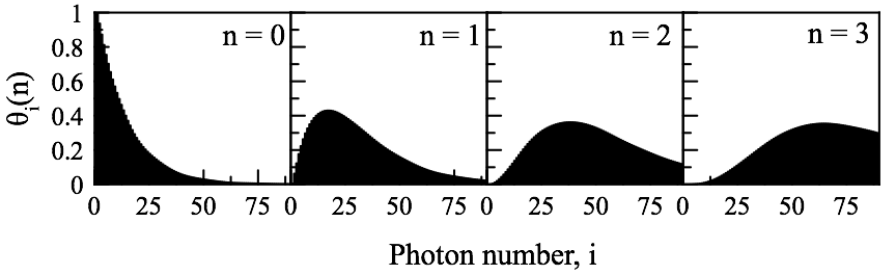

Fig. 5. Diagonal elements of the reconstructed POVM elements for clicks 0, 1, 2 and 3 from a TM-SNSPD (biased at 0.9 × I_C) at λ = 1310 nm at a repetition rate of 4 MHz.

In the POVM reconstruction, we have neglected the effects of dark counts because in the worst-case scenario of TM-SNSPD operation, both the detectors were tuned to operate with a maximum ungated dark count rate of 1 kHz. The experiment's maximum operating rate was 4 MHz and the measurement was time resolved using a FPGA collecting data from 8 time bins of 10 ns each in each clock cycle. The probability of observing a dark count with in the measurement bin was 1.6×10^{-4}. Therefore, the effect of dark counts on the POVM is negligible. Similarly measurement uncertainties in our experiment have been evaluated, but do not have a significant bearing on our data analysis. In the experiment, a calibrated power meter (traceable to the US National Institute of Standards and Technology) was employed. This results in a fixed ± 5% systematic uncertainty in our measurements of the laser power P measured at the transmitted port of the BS. This is the dominant error in our experiment. Systematic error in P will simply add or subtract from efficiency of the detector extracted from the tomographic characterization [24]. Another potential source of error arises from the multinomial or Poissonian distribution of the measurement statistics, which is due to the finite measurement time. The effect of such noise on the tomography result can be estimated from either a Monte-Carlo simulation or by Bayesian inference [39, 40]. We performed a Monte-Carlo simulation based on our measurement data. The simulation results show that the variation in the measurement statistics results in an uncertainty of about 1% in the tomography results.

#175855 - $15.00 USD Received 10 Sep 2012; revised 18 Dec 2012; accepted 18 Dec 2012; published 9 Jan 2013

5. Conclusion

SNSPDs are ideal detectors for optical QIS experiments at telecom wavelengths, having both reasonable quantum efficiency and rapid response with low dark counts. We have presented quantum tomography of TM-SNSPDs with photon resolving capability with the help of a fiber network. The experiments were carried out at the main telecom wavelengths (1310 nm, 1550 nm) at repetition rates of up to 4 MHz, taking into account two polarizations and a range of bias points (0.7-0.9 × I_c). Linear behavior of binary and TM detectors was observed in our experiments, which is confirmed by the reconstructed POVM. In the case of a binary detector, the coefficient of the reconstructed POVM element of the click-event was observed to be zero for the zero-photon component and increases to 1 for higher photon-number components. The detection efficiency calculated from the POVM elements of the best device (Fig. 4(b) and Fig. 3(d)) in our setup had ~18% efficiency at 1550 nm at I_b = 0.9 × I_c. A time-multiplexed detector, as a photon-number-resolving detector, has more outcomes ranging from, for example, no-click to N-clicks. In some of the earlier PNR SNSPD demonstrations such as reference [21], the detectors were operated in the non-linear regime (i.e. biased very low) to study the multiphoton detection statistics. In our experiment, the detectors were biased at 0.9 × I_c and the fiber time multiplexing network was employed to explore the PNR configuration. The POVM element of each outcome gives a distinct sensitive region, which confirms that the detector has a capability to (partially) resolve the input photon number. The POVM element of the N-click event has a similar behavior as that of the click event of a binary detector, showing the response of the detector when it is saturated.

SNSPD device technology is improving rapidly [12]. It is reasonable to foresee construction of a fast, photon number resolving TM-SNSPD, using highly efficient (>50%) SNSPDs, with fast recovery times (~1 ns) integrated on to a waveguide circuit platform. There are also various future paths to be explored in pursuit of a rigorous assumption-free characterization of SNSPDs. Notably, the inclusion of complete wavelength-, polarization- and phase information in the Hilbert-space will give a comprehensive definition of the SNSPD. This method will thus provide a full description of the detection unit in QIS experiments relying on photons.

Acknowledgments

We thank A. Datta, T. J. Bartley, B. J. Smith, J. S. Lundeen for assistance and fruitful discussions. This work is supported by the UK Engineering & Physical Sciences Research Council (EPSRC) (grant numbers EP/H03031X/1 and EP/F048041/1), US EOARD (grant numbers 093020 and FA8655-11-1-3074). CMN acknowledges a SU2P Entrepreneurial Fellowship and RHH acknowledges a Royal Society University Research Fellowship. VZ acknowledges support from FOM, the Netherlands.

#175855 - $15.00 USD Received 10 Sep 2012; revised 18 Dec 2012; accepted 18 Dec 2012; published 9 Jan 2013